# Manganese–polypyrrole–carbon nanotube, a new oxygen reduction catalyst for air-cathode microbial fuel cells

Min Lu [a], Lin Guo [a], Shailesh Kharkwal [a,b], Hua'nan Wu [a,c], How Yong Ng [b], Sam Fong Yau Li [a,c,*]

[a] Department of Chemistry, Faculty of Science, National University of Singapore, 3 Science Drive 3, Singapore 117543
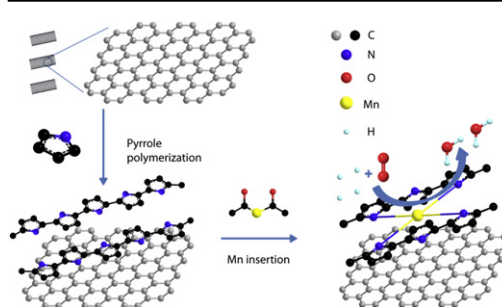[b] Centre for Water Research, Department of Civil and Environmental Engineering, National University of Singapore, 9 Engineering Drive 1, Singapore 117576
[c] NUS Environmental Research Institute, National University of Singapore, 5A Engineering Drive 1, Singapore 117411

## HIGHLIGHTS

► We synthesized cost-effective manganese–polypyrrole–carbon nanotube composite successfully.
► We characterized the manganese–polypyrrole–carbon nanotube composite comprehensively.
► Manganese–polypyrrole–carbon nanotube composite catalyzed oxygen reduction effectively.
► Manganese–polypyrrole–nanotube composite showed good activity as cathode catalyst in air-cathode microbial fuel cells.
► Stability of manganese–polypyrrole–carbon nanotube composite was found to be remarkably good.

## GRAPHICAL ABSTRACT

## ABSTRACT

A novel manganese–polypyrrole–carbon nanotube (Mn–PPY–CNT) composite is synthesized and demonstrated as an efficient and stable cathode catalyst for oxygen reduction reaction (ORR) in air-cathode microbial fuel cells (MFCs). The Mn–PPY–CNT composite is prepared by solvothermal method and comprehensively characterized. Subsequently, electro-catalytic capability of this novel catalyst in neutral electrolyte has been investigated by cyclic voltammetry, showing that Mn–PPY–CNT can catalyze ORR in neutral medium with quite good activity, possibly due to manganese–nitrogen (Mn–N) active sites. To further verify catalytic capability of the Mn–PPY–CNT composite, it has been utilized as the cathode catalyst in air-cathode MFCs. It has been found that Mn–PPY–CNT-based MFCs yield efficient and stable performance with maximum power density of 169 mW m$^{-2}$ at the loading of 1 mg cm$^{-2}$, and 213 mW m$^{-2}$ at the loading of 2 mg cm$^{-2}$, comparable to MFCs with the benchmark platinum/carbon black (Pt/C) catalyst. Furthermore, the catalyst shows good long-term stability which is essential for MFC study. This is the first study regarding the manganese–heterocycle polymer composite as a new ORR catalyst, and it has successfully demonstrated that using cheap Mn–PPY–CNT catalyst instead of Pt/C could improve the feasibility of scaling up MFCs for practical applications.

© 2012 Elsevier B.V. All rights reserved.

* Corresponding author. Department of Chemistry, Faculty of Science, National University of Singapore, 3 Science Drive 3, Singapore 117543. Tel.: +65 6516 2681; fax: +65 6779 1691.
E-mail address: chmlifys@nus.edu.sg (S.F.Y. Li).

## 1. Introduction

Microbial fuel cell (MFC), a device to convert biomass energy in wastewater into bioelectricity, has attracted much attention in the

past decades. Normally, an MFC comprises a cathode, a separator and a bioanode. Electrogenic bacteria form a biofilm on anode surface at the inoculation stage, degrading organic matters in wastewater for electron and proton generation. Electrons migrate through the external circuit to cathode where electron acceptors get reduced by accepting electrons, and meanwhile protons migrate in the internal circuit across the separator to complete a whole circuit [1]. The unique property of MFC shows great promise in harvesting energy from waste material [2], bioremediation for pollutant control [3,4], desalination for fresh water generation [5,6], chemical production [7,8] and also application as sensing systems [9]. Nevertheless, there still remain many challenges such as improving the power output, scaling up, and lowering the capital cost [10].

To achieve higher electricity output, cathode is one of the key aspects with potential for improvement [11]. Among various cathode candidates, oxygen has been mostly chosen as the electron acceptor because of its abundance, sustainability and high reduction potential [12]. Nevertheless, the slow kinetics of oxygen reduction reaction (ORR) restricts the performance of the oxygen cathode, and catalysts are conventionally required. Platinum (Pt)-based catalysts are commonly used to improve ORR performance because of their high efficiency. Unfortunately, the high price and low reserve of Pt limit the further scaling up of MFCs. The exploration of efficient noble metal free catalysts is urgently required. To this end, modified carbon materials [13], metal oxides [14,15] and iron (Fe), cobalt (Co)-heterocycles [16,17] have been investigated as potential ORR catalysts. In addition, manganese–porphyrin [18] and manganese oxides–polypyrrole composites prepared by electro-polymerization [19,20] have been reported to possess good ORR catalytic capability in the unconventional electrolyte (benzoic anhydride) [18] or acidic environment [19,20] respectively. Polypyrrole-containing composite [21] is tested on MFCs with the assumption that carbon atoms on pyrrole ring could supply an active site for oxygen chemical adsorption to decrease the activation energy. Nevertheless, few of them have been demonstrated to possess both good activity and long-term stability in a neutral MFC environment. In this study, manganese–polypyrrole–carbon nanotube composite is synthesized with expectation of manganese–nitrogen (Mn–N) interaction (Scheme 1), creating active sites for ORR catalysis [22]. Subsequently, the as-synthesized catalyst is further applied on MFC cathode. The composite shows comparable catalytic capability to Pt-based catalysts, and it would further facilitate the scaling up of MFCs.
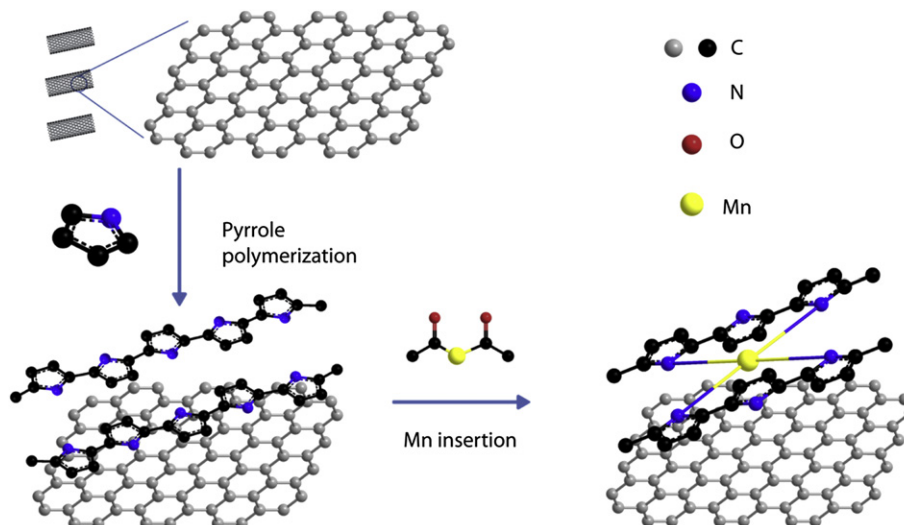
## 2. Experimental

### 2.1. Preparation of manganese–polypyrrole–carbon nanotube composite

The sample preparation includes two processes as in-situ chemical polymerization and in-situ Mn deposition. Briefly, carbon nanotubes (CNTs, Shenzhen Nanotech Port Co. Ltd, with the outer diameter of 60–100 nm, purity > 97%, ash < 3%) are firstly washed with 5% $HNO_3$ followed by deionized (DI) water to remove impurities and dried under vacuum at 70 °C. 0.2 g $HNO_3$-treated CNTs are added into 100 mL dimethylformamide (DMF), ultrasonicated and stirred overnight for better dispersion. Subsequently, 1 mL acetic acid (which serves to maintain an acidic environment for in-situ polymerization, and as dopant to improve conductivity of polypyrrole) is added into the mixture under vigorous stirring, and 1 mL distilled pyrrole is added 30 min later. To the resulting mixture, 2 mL of hydrogen peroxide is added dropwisely, which is then kept at room temperature (~25 °C) for 3 h. Upon the addition of 1.0 g manganese (II) acetate ($MnAc_2$, excess) to the reaction mixture, temperature is rapidly increased to 180 °C and maintained for 24 h. Finally, the product is filtered, washed and dried under vacuum at 70 °C. The black powder obtained is named manganese–polypyrrole–carbon nanotube (Mn–PPY–CNT).

Several other composites are also prepared as controls: 1). Polypyrrole (PPY) is prepared by in-situ polymerization using the same method described above without the addition of CNTs or $MnAc_2$. 2). PPY–CNT is prepared using the same method described above only without addition of $MnAc_2$. 3). Mn–CNT is prepared using the same method described above only without addition of pyrrole monomer.

The N content of these composites, as an indicating parameter for PPY loading is determined by elemental analysis (Elementar Vario Micro Cube). Inductively coupled plasma-optical emission spectrometry (ICP-OES, Dual-view Optima 5300 DV) is applied to determine the overall Mn element, while X-ray photoelectron spectroscopy (XPS, Kratos AXIS Ultra$^{DLD}$) is employed to measure



**Scheme 1.** Schematic representation of the preparation procedure for manganese–polypyrrole–carbon nanotube composite.

the surface elemental content of Mn. PPY polymerization is confirmed by Fourier transform infrared spectrophotometer (FTIR, Shimadzu IRPrestige-21), and the degree of polymerization is examined by gel permeation chromatography (GPC, Waters e2695 separation modules with Waters 2414 refractive index detector) in tetrahydrofuran. Conductivity measurements of the composites are made on pressed pellets (1.3 cm diameter, <1 mm thickness) measured by a conventional four-probe technique with an SD-600 sheet resistivity meter. Morphological characterization of the composites is conducted on field-emission scanning electron microscope (SEM, JEOL JSM-6701F) at an acceleration voltage of 5.0 kV. The prepared composites are ground in an agate mortar before each test. All the chemical reagents are analytical pure and used without further purification unless otherwise specified.

## 2.2. Electrode fabrication

The electrodes with catalyst coating are fabricated with 5% Nafion solution as the binder. Briefly, composites are mixed with the Nafion solution and dispersed well by ultrasonication. A small volume of slurry is extracted and coated on the surface of glass carbon electrode (GCE, with a diameter of 3.0 mm) by a micropipette. The GCEs are dried in air at room temperature to remove the solvent. Pt/C-coated GCEs are similarly prepared.

## 2.3. Electrochemical measurement

Electrochemical analysis of the composite is done by cyclic voltammetry (CV) using a potentiostat (IVIUMSTAT) with a three-electrode system where GCE coated by catalyst (Mn−PPY−CNT or Pt/C) serves as the working electrode, Ag/AgCl/KCl (3 M) and a Pt mesh electrode are used as the reference and counter electrode, respectively. CV is taken between 0.2 V and −1.0 V at 50 mV s$^{-1}$ in 0.2 M NaCl electrolyte. The electrolyte solution is bubbled with O$_2$ or N$_2$ to establish aerobic or anaerobic environment respectively for 30 min prior to each scan series, and 3 min between every two scans.

## 2.4. Air-cathode MFC set-up

The MFCs used are the same reactors as previously reported [14]. Generally, acrylic single-chamber MFC reactors with the anodic chamber of $\Phi$ 6 cm × 1 cm (28.3 mL) are assembled. Non-wet proof carbon clothes (E-TEK) are used as anodes, and also as the cathodes (28.3 cm$^2$) after modification. The carbon base layer and cathode catalysts are coated onto the cathode carbon cloth by subsequently spraying slurries and dried at room temperature. The resulting cathode carbon cloth with carbon base layer and catalyst layer at the inner side is then hot pressed together with the proton exchange membrane (PEM, Nafion 117) to form the membrane-cathode-assembly [23]. In this study, cathodes with different catalysts and different loadings, Pt/C (0.5 mg Pt cm$^{-2}$), Mn−PPY−CNT (1 mg cm$^{-2}$) and Mn−PPY−CNT (2 mg cm$^{-2}$), are used in MFCs as duplicates respectively.

Activated sludge (Ulu pandan water reclamation plant, Singapore) is used as inoculum at the beginning, and artificial wastewater (~1 g L$^{-1}$ sodium acetate in 30 mM phosphate saline buffer with mineral and vitamins solution [24]) is applied as anolyte, fed continuously at a flow rate of 1.3 mL min$^{-1}$ after successful inoculation. A 10 $\Omega$ resistor is connected to each MFC, and voltage across the resistor is constantly monitored for four months and recorded at a fixed interval by a home-made data acquisition system (DAS). Currents are obtained by measuring voltages across

different resistors and polarization curves are plotted after further calculation.

## 3. Results and discussion

### 3.1. Synthesis and characterization of the catalysts

The Mn−PPY−CNT composite is synthesized as shown in Scheme 1. PPY is firstly in-situ polymerized in the presence of CNTs. Subsequently, Mn is deposited onto the PPY at elevated temperature. To demonstrate successful synthesis of the novel catalyst, polymerization of pyrrole is verified. PPY is synthesized in the absence of CNTs under the same conditions to eliminate the interference of CNTs on the characterization of PPY. The FTIR spectrum of this as-synthesized PPY (Fig. S1) has the characteristic peaks (3394 cm$^{-1}$ for N−H stretching, 3232 cm$^{-1}$ for C−H stretching, 1697 cm$^{-1}$ for C=C stretching, 1396 cm$^{-1}$ and 1365 cm$^{-1}$ for C−C and C−N in-plane stretching, 1288 cm$^{-1}$, 1195 cm$^{-1}$, 1110 cm$^{-1}$ for C−H deformation and ~763, 648, 547 cm$^{-1}$ for ring torsion), demonstrating the sample to be PPY [25]. To further confirm PPY polymerization, gel permeation chromatography is applied to determine the average molecule weight of the resultant product. As expected, the result (weight average molecule weight = 105,430 ± 782 g mol$^{-1}$) indicates successful polymerization at high degree.

The Mn−PPY−CNT composite is further characterized with elemental analysis to identify the presence of Mn. The elemental contents of the composites are summarized in Table 1. It can be seen that Mn is present in the Mn−PPY−CNT composite with a loading of 0.15%. A further XPS study shows that the as-synthesized catalyst has a surface Mn content of 0.5% (Fig. S2). The disparity of the two values is attributable to the fact that ICP-OES determines the overall Mn content in the composite while XPS measures the surface Mn content within the depth of several nanometers. Therefore the higher value of surface Mn content with the presence of CNTs indicates the dispersion of Mn on the outer surface of CNTs.

Conductivity is an essential parameter for electrocatalysts, which could largely affect the catalytic performance. As summarized in Table 1, Mn−PPY−CNT composite has a high conductivity ($\sigma$ = 138.45 Sm$^{-1}$). Comparing with PPY−CNT, Mn−CNT, raw and HNO$_3$-treated CNTs, it is believed that the higher conductivity of Mn−PPY−CNT is because of synergistic effect of the metal and conductive polymer. The composite is further characterized under SEM. As shown in Fig. 1, no significant difference in morphology has been observed in the SEM images for Mn−PPY−CNT (Fig. 1A), PPY−CNT (Fig. 1C), and HNO$_3$-treated CNT (Fig. 1D), indicating that Mn could be uniformly inserted onto PPY−CNT composite. In stark contrast, obvious aggregates appear when depositing Mn onto CNTs in the absence of PPY (Fig. 1B), and these aggregates are identified as Mn$_3$O$_4$ (Fig. S3). The resulting Mn−CNT composite has even lower conductivity while comparing with raw CNTs. These results further indicate the significance of the interaction between PPY and Mn.

**Table 1**
Elemental content (N, Mn) and conductivity for Mn−PPY−CNT and other composites. Note: wt% represents weight−weight percentage.

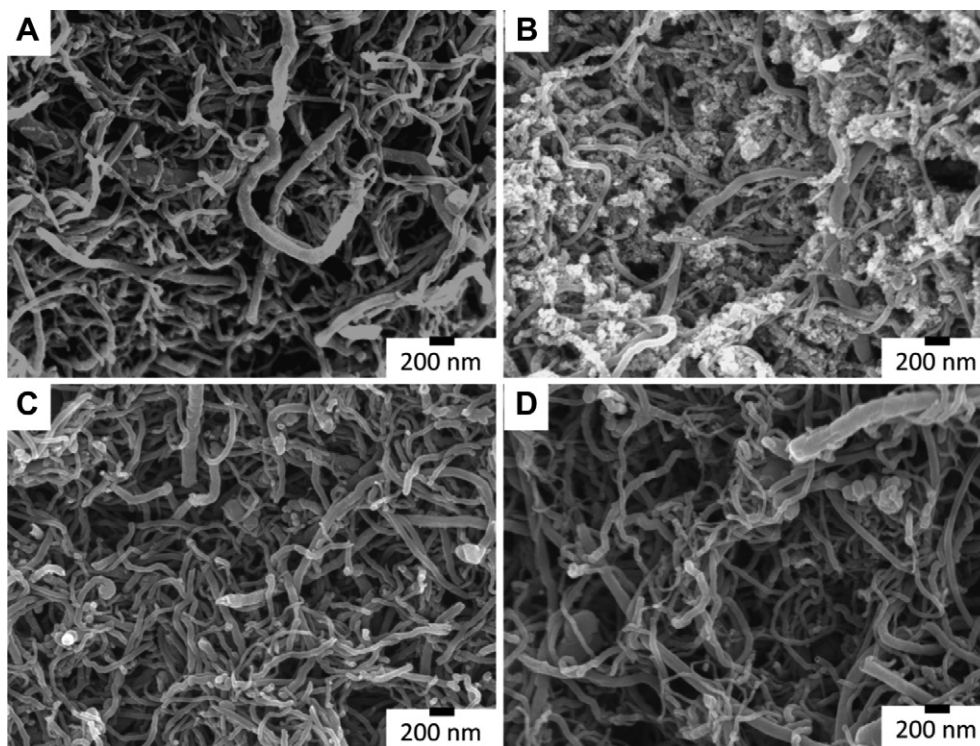| Sample | N/wt% | Mn/wt% | Conductivity/Sm$^{-1}$ |
|---|---|---|---|
| Mn−PPY−CNT | 3.42 | 0.15 | 138.45 |
| Mn−CNT | <0.50 | 44.87 | 41.35 |
| PPY−CNT | 1.39 | − | 71.87 |
| HNO$_3$-treated CNT | 0.96 | − | 75.51 |
| Raw CNT | <0.50 | − | 45.01 |

**Fig. 1.** Morphology for composites prepared by solvothermal method. A) Mn−PPY−CNT, B) Mn−CNT, C) PPY−CNT, D) HNO₃-treated CNT.

### 3.2. Electrochemical characterization of Mn−PPY−CNT composite

The catalytic property of the Mn−PPY−CNT composite is first tested by cyclic voltammetry under aerobic and anaerobic environments (Fig. 2). Herein, the benchmark Pt/C catalyst is used to identify the reduction peak of ORR process. As shown in Fig. 2, the benchmark Pt/C catalyst possesses a broad reduction peak (−0.2 to −0.4 V) at high onset potential in aerobic environment (Fig. 2f) but no peak in anaerobic environment (Fig. 2g), indicating the peak attribution to the catalyzed ORR process.
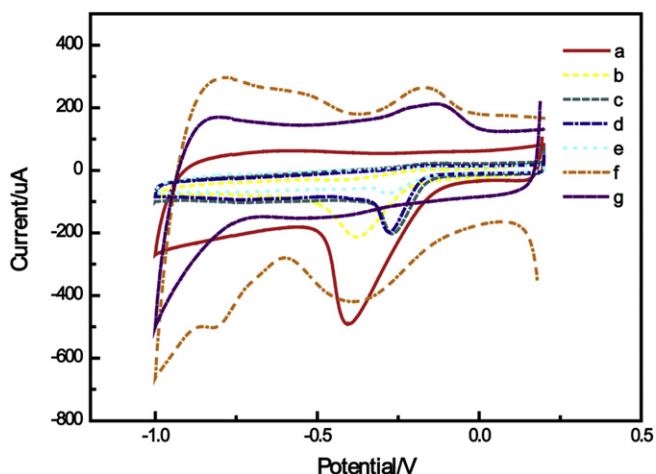


**Fig. 2.** Cyclic voltammograms for ORR in 0.2 M NaCl solution between 0.2 and −1.0 V at the scan rate of 50 mV s⁻¹ with different catalysts and conditions. a) Mn−PPY−CNT with loading of 1 mg cm⁻²; b) Mn−CNT with loading of 1 mg cm⁻²; c) PPY−CNT with loading of 1 mg cm⁻²; d) HNO₃-treated CNTs with loading of 1 mg cm⁻²; e) raw CNTs with loading of 1 mg cm⁻²; f) Pt/C with loading of 0.5 mg Pt cm⁻²; g) Pt/C with loading of 0.5 mg Pt cm⁻², (a−f) are operated in aerobic condition, and (g) is operated in anaerobic condition.

Comparing with Pt/C catalyst, raw CNTs (Fig. 2e) possess a small ORR peak, and there is a big improvement after HNO₃ treatment (Fig. 2d), which could be because of the increased conductivity (Table 1) and also the defects (N replacement of C in the carbon backbone) induced by HNO₃ treatment [26]. Nevertheless, the performance of the sole CNTs cannot meet the requirement of efficient ORR catalysis. Subsequently, Mn−PPY−CNT is examined in the identical conditions. Inspiringly, after in-situ PPY polymerization and Mn insertion in DMF, the Mn−PPY−CNT (Fig. 2a) shows increased ORR catalytic performance, indicated by the comparable peak current to Pt/C. In contrast, neither PPY polymerization (Fig. 2c) nor Mn insertion (Fig. 2b) independently shows any obvious improvement to the catalytic performance of CNTs, indicating a fact that the increased catalytic capability is attributed to synergistic effect of PPY and Mn. In addition, it is found that the reaction condition is crucial for the synthesis of efficient catalysts. For example, when ethanol is applied as the solvent, the resultant Mn−PPY−CNT composite prepared at lower temperature does not show any improvement under CV characterization (Fig. S4B) despite the similar morphology (Fig. S4A) and similar metal content (∼1‰). It is thus proposed that the catalytic capability is related to Mn−N interaction [22]. Normally, the interaction between Mn atom and N-heterocycle is a thermodynamically unfavorable reaction with unstable product, and harsh conditions are needed [27]. Consequently, the reaction using DMF as the solvent with high refluxing temperature would produce Mn−PPY−CNT composite with better catalytic capability. To further investigate the catalytic mechanism of Mn−PPY−CNT prepared in DMF, scan rates for CV were varied. The linear relation obtained between peak current and square root of scan rate indicates the ORR catalyzed by Mn−PPY−CNT catalyst is a diffusion-controlled process (Fig. S5). According to the Randles−Sevcik equation [28], the number of electrons transferred is calculated to be 2.87, and therefore the catalytic mechanism is proposed as follows [22]:
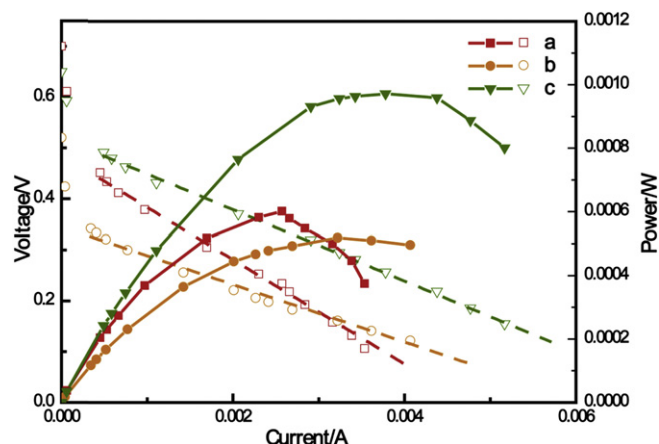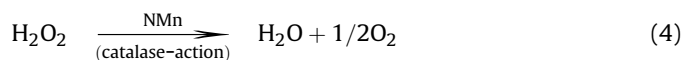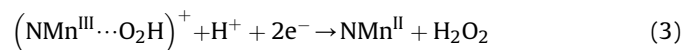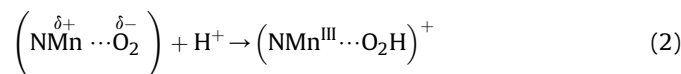
**Fig. 3.** Polarization and power curves for air-cathode MFCs respectively when MFCs have reached their performance stabilization. Cell voltage ($E$) data are collected by data acquisition system across different external resistance ($R_{ex}$), subsequently current and power are calculated using $R_{ex}$ and E. Voltage and power are plotted as functions of the current to make polarization and power curves, respectively. The dash lines with empty symbols are polarization curves and the solid lines with close symbols are power curves. a) Mn–PPY–CNT catalyst (2 mg cm$^{-2}$), b) Mn–PPY–CNT catalyst (1 mg cm$^{-2}$) and c) Pt/C catalyst (0.5 mg Pt cm$^{-2}$).

$$NMn^{II} + O_2 \rightleftarrows \left( N\overset{\delta+}{Mn} \cdots \overset{\delta-}{O_2} \right) \qquad (1)$$

$$\left( N\overset{\delta+}{Mn} \cdots \overset{\delta-}{O_2} \right) + H^+ \rightarrow \left( NMn^{III} \cdots O_2H \right)^+ \qquad (2)$$

$$\left( NMn^{III} \cdots O_2H \right)^+ + H^+ + 2e^- \rightarrow NMn^{II} + H_2O_2 \qquad (3)$$

$$H_2O_2 \xrightarrow[\text{(catalase-action)}]{NMn} H_2O + 1/2O_2 \qquad (4)$$

### 3.3. MFC performances with various catalysts

To further demonstrate the catalytic capability of Mn–PPY–CNT composite for ORR, Mn–PPY–CNT composite is then applied in MFCs as cathode catalyst. For comparison, Pt/C catalyst is used as benchmark control. As shown in Fig. 3 and Table 2, the MFCs with Mn–PPY–CNT catalysts (1 mg cm$^{-2}$) produce satisfactory power output in terms of maximum power density ($P_{max}$ = 169 mW m$^{-2}$) and open circuit potential (OCV = 0.52 V), comparable to that of Pt/C catalyst. When Mn–PPY–CNT loading amount is increased (2 mg cm$^{-2}$), the OCV (0.70 V) and $P_{max}$ (213 mW m$^{-2}$) of MFCs are increased as desired. Inspiringly, this quasi-metal free catalyst

**Table 2**
Summary of air-cathode MFC performances with different catalysts when the MFCs have reached their performance stabilization.

| Catalysts | Open circuit voltage (V) | Internal resistance ($\Omega$) | Maximum power (mW) | Maximum power density (mW m$^{-2}$) |
|---|---|---|---|---|
| Mn–PPY–CNT (2 mg cm$^{-2}$) | 0.70 | 103 | 0.602 | 213 |
| Mn–PPY–CNT (1 mg cm$^{-2}$) | 0.52 | 56 | 0.478 | 169 |
| Pt/C (0.5 mg Pt cm$^{-2}$) | 0.65 | 70 | 0.971 | 343 |

($\sim 1\permil$ Mn for Mn–PPY–CNT) possesses good stability. After four months of operation, the maximum power densities of Mn–PPY–CNT-based MFCs were 214 mW cm$^{-2}$ (loading of 2 mg cm$^{-2}$), and 153 mW cm$^{-2}$ (loading of 1 mg cm$^{-2}$), with less than 10% decrease in terms of $P_{max}$, demonstrating the feasibility of Mn–PPY–CNT catalyst for long-term application with low cost and low possibility for metallic pollution in practical applications.

## 4. Conclusion

In this study, a novel Mn–PPY–CNT composite is synthesized, characterized, investigated by CV method in neutral medium and finally incorporated into the air-cathode MFCs as cathode ORR catalyst. It is shown that Mn–PPY–CNT composite has quite good capability for ORR catalysis in neutral medium. When Mn–PPY–CNT catalysts are applied onto air-cathode MFCs, the performance of Mn–PPY–CNT-based MFCs is comparable to that of Pt/C-based MFCs. Furthermore, stability of this catalyst is quite satisfactory.

This is the first study regarding manganese–polypyrrole–carbon nanotube composite for ORR catalysis and would contribute to exploration of this new category of ORR catalyst. Due to its low cost, low metallic content, easy preparation, good MFC performance and long-term stability, Mn–PPY–CNT catalyst could be a very promising electrocatalyst for air-cathode MFCs. It is believed that that this efficient and economic catalyst could facilitate the scaling up and commercialization of MFC reactors for practical applications.

## Appendix A. Supplementary material

Supplementary material associated with this article can be found, in the online version, at http://dx.doi.org/10.1016/j.jpowsour.2012.08.034.

## References

[1] B.E. Logan, Microbial Fuel Cells, John Wiley & Sons, Inc., Hoboken, New Jersey, 2008.
[2] S. Puig, M. Serra, M. Coma, M. Cabre, M. Dolors Balaguer, J. Colprim, Journal of Hazardous Materials 185 (2011) 763–767.
[3] L. Huang, J. Chen, X. Quan, F. Yang, Bioprocess and Biosystems Engineering 33 (2010) 937–945.
[4] J.C. Thrash, J.I. Van Trump, K.A. Weber, E. Miller, L.A. Achenbach, J.D. Coates, Environmental Science & Technology 41 (2007) 1740–1746.
[5] F. Zhang, K.S. Brastad, Z. He, Environmental Science & Technology 45 (2011) 6690–6696.
[6] X. Cao, X. Huang, P. Liang, K. Xiao, Y. Zhou, X. Zhang, B.E. Logan, Environmental Science & Technology 43 (2009) 7148–7152.
[7] X. Wang, Y. Feng, J. Liu, H. Lee, C. Li, N. Li, N. Ren, Biosensors and Bioelectronics 25 (2010) 2639–2643.
[8] L. Fu, S. You, F. Yang, M. Gao, X. Fang, G. Zhang, Journal of Chemical Technology & Biotechnology 85 (2010) 715–719.
[9] I.S. Chang, H. Moon, J.K. Jang, B.H. Kim, Biosensors and Bioelectronics 20 (2005) 1856–1859.
[10] K. Rabaey, L. Angenent, U.K.S. Schroder, Bioelectrochemical Systems: From Extracellular Electron Transfer to Biotechnological Application, IWA Publishing, 2009.
[11] M. Lu, S.F.Y. Li, Critical Reviews in Environmental Science and Technology, in press.
[12] F. Harnisch, U. Schroder, Chemical Society Reviews 39 (2010) 4433–4448.
[13] H.M. Wang, Z.C. Wu, A. Plaseied, P. Jenkins, L. Simpson, C. Engtrakul, Z.Y. Ren, Journal of Power Sources 196 (2011) 7465–7469.
[14] M. Lu, S. Kharkwal, H.Y. Ng, S.F.Y. Li, Biosensors and Bioelectronics 26 (2011) 4728–4732.
[15] Y. Zhang, Y. Hu, S. Li, J. Sun, B. Hou, Journal of Power Sources 196 (2011) 9284–9289.

[16] R. Bashyam, P. Zelenay, Nature 443 (2006) 63–66.
[17] K.N. Zhu, H.Y. Qin, B.H. Liu, Z.P. Li, Journal of Power Sources 196 (2011) 182–185.
[18] N.P. Rodrigues, J. Obirai, T. Nyokong, F. Bedioui, Electroanalysis 17 (2005) 186–190.
[19] H.N. Cong, K. El Abbassi, J.L. Gautier, P. Chartier, Electrochimica Acta 50 (2005) 1369–1376.
[20] K. Ding, F. Cheng, Synthetic Metals 159 (2009) 2122–2127.
[21] Y. Yuan, S. Zhou, L. Zhuang, Journal of Power Sources 195 (2009) 3490–3493.
[22] F. Beck, Journal of Applied Electrochemistry 7 (1977) 239–245.
[23] S. Cheng, H. Liu, B.E. Logan, Electrochemistry Communications 8 (2006) 489–494.
[24] D.R. Lovley, E.J.P. Phillips, Applied and Environmental Microbiology 54 (1988) 1472–1480.
[25] B. Tian, G. Zerbi, Journal of Chemical Physics 92 (1990) 3886–3891.
[26] N. Duteanu, B. Erable, S.M. Senthil Kumar, M.M. Ghangrekar, K. Scott, Bioresource Technology 101 (2010) 5250–5255.
[27] A.D. Adler, F.R. Longo, F. Kampas, J. Kim, Journal of Inorganic and Nuclear Chemistry 32 (1970) 2443–2445.
[28] A.J. Bard, L.R. Faulkner, Electrochemical Methods: Fundamentals and Applications, second ed., John Wiley & Sons, Inc., 2000.